

Structural stability and uniformity of magnetic Pt₁₃ nanoparticles in NaY zeolite

Cono Di Paola¹, Luca Pavan¹, Roberto D’Agosta^{*2,3}, and Francesca Baletto^{†1}

¹Department of Physics, King’s College London, London, WC2R 2LS, United Kingdom

²Nano-bio Spectroscopy Group and ETSF Universidad del Pais Vasco, CFM CSIC-UPV/EHU, E-20018 Donostia-San Sebastian, Spain

³IKERBASQUE, Basque Foundation for Science, E-48013 Bilbao, Spain

September 2, 2017

Numerical Methodology

Metadynamics (MT) is an algorithm used to accelerate rare events, where the ionic dynamics is biased by a history-dependent potential built on a set of reaction coordinates called collective variables (CVs).¹ Commonly used to explore free-energy surfaces, MT has been recently proposed for sampling the energy landscape of small clusters.² An analytic coordination number (CN) is employed, and the meta-potential is constructed by adding Gaussian functions of 5 meV every 15 ps. Each independent simulation has a minimum length of 2 μ s and is performed at 5 ± 2 K. The analytic coordination number (CN) of a cluster is a geometry-related variable defined as the sum of the total number of nearest neighbours of each atom,

$$\begin{aligned} CN &= \sum_{i,j} f(x_{ij}) \\ x_{ij} &= \frac{r_{ij} - d_0}{r_0} \\ f(x_{ij}) &= \begin{cases} 1 & \text{if } r_{ij} < d_0 \\ \frac{1 - x_{ij}^n}{1 - x_{ij}^m} & \text{if } r_{ij} > d_0 \end{cases} \end{aligned} \quad (1)$$

where d_0 is the nearest neighbour bulk reference distance, r_0 is a distance related to the width of the descending branch of the function, n and m are parameters used for tuning its smoothness and asymptotic behaviour. The best choice turns to be $m = 12, n = 6, r_0 = 0.15d_0$. The starting configurations are taken among the suggested best minima reported in the literature, such as BP, TBP, TP, and LOW structures and well-known geometries such as icosahedron (Ih), cubooctahedron (Co) and decahedron (Dh). To ensure a detailed search, an iterative procedure (iMT) is applied. When a morphology belonging to a new structural basin is gained, it is quenched to its nearest local minimum and then used as initial position for a new run in an iterative manner.³ To speed up the search, the atomic interactions are described by an empirical potential (EP) derived in the second-moment approximation of tight binding.⁴ The use of EP-iMT is justified by the need to efficiently identify the largest possible ensemble of highly coordinated local minima. The adopted EP is demonstrated to provide the correct geometrical details of transition metal NPs, with the exception of those with small Jahn-Teller distortions. Nonetheless, the relative energy stability of each isomer is calculated according to the Broyden-Fletcher-Goldfarb-Shanno (BFGS) algorithm after ionic relaxation, within a scalar-relativistic spin-polarized DFT framework, as available in the Quantum Espresso package.⁵ Scalar-relativistic spin-polarised calculations are able to reproduce correctly the geometrical features and the magnetic moment of Pt₁₃ with respect to relativistic approaches, including spin-orbit coupling.⁶ The Perdew-Burke-Ernzerhof exchange-correlation functional and ultrasoft pseudo-potential with a Pt

*roberto.dagosta@ehu.es

†francesca.baletto@kcl.ac.uk

electronic configuration $5d^9 6s^1$ are used with an energy and a charge density cutoff of 612.26 eV and 4898.05 eV, respectively. A non-linear core correction is also included. All the calculations are performed at Γ point, and a Marzari-Vanderbilt smearing of 0.03 eV is applied.⁷ The degeneracy of magnetic states of a few free Pt-NPs as BP, TBP and Ih was checked performing constrained spin-polarised simulations as reported in.⁸ Although the Ih is almost degenerate up to $S = 3$, it remains very high in energy. The TBP has almost degenerate magnetic states up to $S = 3$, and an energy crossing with the BP is observed when the spin states are between 3 and 4. In the case of free NPs, the simulation box contains at least 13 Å of vacuum to avoid any spurious interaction between periodic images. In the case of embedded NPs in the $H_{30}O_{42}Al_6Si_{24}$ cage, a cubic cell of approximately 28 Å is used and a full BFGS ionic relaxation is applied to Pt atoms and the three inward oxygen atoms of the six-ring substructure. Both standard DFT and corrected DFT for van der Waals forces (DFT-D), where a semi-empirical damp-dispersion term is introduced,⁹ are performed. The NaY supercage does not exhibit any magnetic behaviour.

Structures of the isomers

In Fig. S1, we report the 14 isomers that could fit into the NaY cage, according to their geometrical families. The description of the different structures, their energy stability, and total magnetization have been discussed in the main paper to which we refer the reader.

The adopted zeolite supercage

Zeolites, which have been known for almost 250 years, are crystalline microporous solids; they have been widely used in chemical industrial applications since their synthesis in the late 1940s. Today, approximately 180 different zeolite frameworks are available as adsorbents, selective catalysts, and ion-exchanger medias. Aluminosilicate zeolites possess a three-dimensional arrangement of AlO_4^- tetrahedra sharing oxygen ions to form subunits that can be periodically repeated. Their general formula is $M_{x/n}(AlO_2)_x(SiO_2)_y$, where n is the valence of the cation, $x + y$ is the total number of tetrahedra per unit cell and y/x is the atomic Si/Al ratio, which is > 1 . In particular, the faujasite (FAU) framework consists of sodalite cages (truncated octahedra) linked through hexagonal prisms or double oxygen six-ring structures; pores are arranged perpendicular to each other. Each pore is formed by a twelve-membered ring with a diameter of 7.4 Å; this ring is interconnected to four neighbouring cages leaving an inner cavity of 12-13 Å, in diameter that is surrounded by 10 sodalite cages. The counterions in faujasite are then distributed among different types of sites, depending on the Si/Al ratio.

To mimic a faujasite supercage environment, a full-silicon model ($H_{36}O_{42}Si_{30}$) and a 1:4 Al/Si model ($H_{30}O_{42}Al_6Si_{24}$) with at least two aluminium atoms per six-ring subunit have been taken in consideration. The crystalline structure is that proposed in the accredited database of zeolite structures (<http://www.iza-structure.org/databases/>). The suggested model has an available volume of 839 Å³, where the available volume is defined as the volume accessible to a spherical molecule after the van der Waals atomic sphere volumes are subtracted from the unit cell. When the Pt-O bond length is taken into account, this available volume indicates that an object with a maximum diameter of 7-8 Å, can be inserted. A selection of Pt₁₃ was inserted in both faujasite models, as depicted in Fig. S2. In all cases, the cluster was chemisorbed through only one vertex at the site II observed in front of the six-ring substructure, which has been suggested to be the most occupied site inside the supercage.¹⁰ Notice that as a reference energy we have taken the one of the Z1-a in the zeolite cage.

With respect to the Si/Al ordering in the zeolite, two models have been considered: one that allows Al-O-Al bridges and the other respecting Löwenstein's rule, where only Si-O-Al fragments occur. In previous DFT studies,¹¹ a periodically repeated Löwenstein's model was observed to be only slightly energetically more favourable than the Al-O-Al sequence. A cubic cell of 28 Å, was selected, and the electronic relaxations in a spin-polarised framework showed no magnetic behaviour for either model. However, having considered only one zeolite supercage, calculations at both the DFT and DFT-D levels revealed that the Al-O-Al fragment was comparable in energy with respect to a Al-O-Si ordering (the latter is lower in energy by about 0.2 eV). Moreover, some of the clusters (D0R-c, D0 and D1, see later) were inserted into the two Si/Al models. Their energy stability and their total magnetisation were not affected by a different order of Al atoms in the ring. However, we have noticed that the

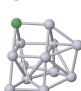

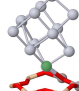
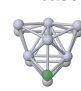
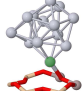
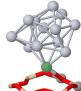

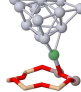
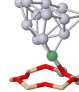
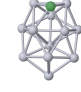
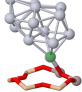
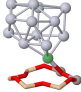
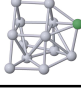
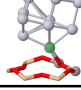
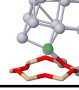
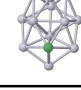
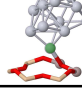
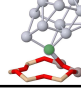
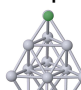
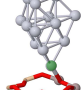
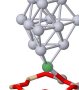
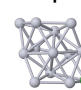

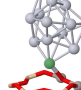
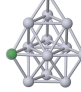
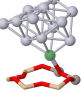
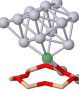
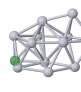
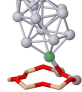

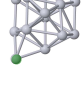
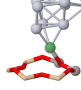
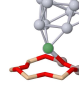
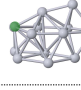
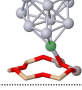
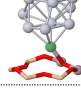
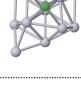
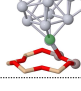
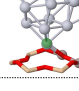
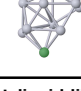
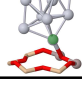
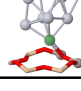
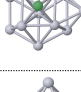
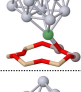
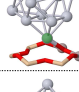
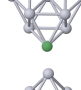
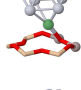
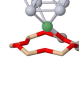
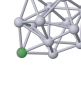
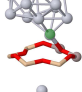
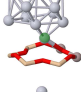
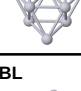
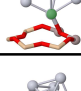
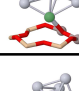
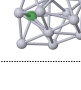
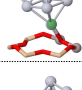
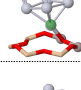
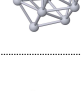
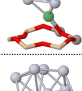
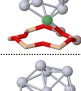
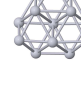
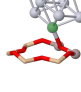
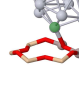
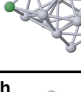
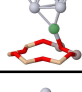
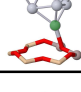
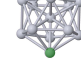
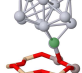
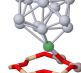
LOW				TTP based							
	F0 2.0 0.00 $\Omega=1.2$ (3)		Z0-a 2.0 0.22 1.1 (3)		D0R-a 2.0 0.65 1.1 (3)		F2 6.0 1.18 $\Omega=1.2$ (4)		Z2 6.0 1.20 1.2 (4)		D2 6.2 2.66 1.3 (4)
	$\Omega=0.8$ (3)		Z0-b 2.0 0.07 0.7 (3)		D0-b 1.9 0.41 1.0 (3)		F6 8.0 1.43 $\Omega=1.4$ (4)		Z6 8.0 1.47 1.3 (4)		D6R* 2.1 0.96 1.6 (4)
	$\Omega=1.2$ (4)		Z0-c 2.0 0.00 1.1 (4)		D0R-c 2.0 0.00 1.0 (3)		$\Omega=2.4$ (5)		Z6R 5.2 0.89 0.8 (3)		D6RR 3.5 0.98 1.0 (3)
Incomplete Dh₂₃				Incomplete d-Ih₁₉							
	F1 6.0 0.41 $\Omega=0.7$ (3)		Z1-a 6.0 0.40 0.7 (3)		D1-a 5.9 1.77 0.8 (3)		F5 8.1 0.75 $\Omega=1.3$ (4)		Z5 8.0 0.80 1.2 (4)		D5 8.0 2.29 1.0 (4)
	$\Omega=1.3$ (4)		Z1-b 5.7 0.48 1.3 (4)		D1-b 6.0 1.97 1.2 (4)		F7 6.0 1.54 $\Omega=1.3$ (4)		Z7 6.0 1.44 1.2 (4)		D7 7.8 2.34 1.5 (4)
	F3 6.2 0.81 $\Omega=0.6$ (3)		Z3-a 4.0 0.58 0.6 (3)		D3-a 3.6 1.41 0.6 (3)		$\Omega=2.6$ (5)		Z7R 4.0 1.06 1.3 (4)		D7RR 2.1 1.06 1.3 (4)
	$\Omega=1.3$ (4)		Z3-b 3.9 0.57 1.3 (4)		D3-b 3.8 1.55 1.4 (4)		F12 6.1 1.48 $\Omega=1.2$ (4)		Z12 6.0 1.26 1.2 (4)		D12 6.0 1.48 1.3 (4)
	F4 4.1 0.71 $\Omega=1.2$ (4)		Z4 2.0 0.76 1.2 (4)		D4 2.1 1.56 1.3 (4)	Helicoid-like					
	F13 5.9 1.34 $\Omega=1.3$ (4)		Z13 4.0 1.33 1.3 (4)		D13 4.1 2.32 1.5 (4)		F8 5.8 1.46 $\Omega=1.4$ (4)		Z8 6.2 1.54 1.3 (4)		D8 2.0 2.47 1.5 (4)
	$\Omega=1.8$ (5)		Z13R 4.0 1.45 1.2 (4)		D13R 4.0 1.46 1.3 (4)		$\Omega=2.4$ (5)		Z8R 4.0 0.91 1.2 (4)		D8RR 4.1 1.15 1.3 (4)
BL					F10 8.0 1.47 $\Omega=0.6$ (3)		Z10 8.0 1.45 0.7 (3)		D10R 6.0 2.46 1.6 (4)		
	F9 2.0 1.20 $\Omega=2.0$ (5)		Z9 2.0 1.34 1.9 (5)		D9 2.0 2.48 2.2 (5)		F11 7.9 1.42 $\Omega=0.6$ (3)		Z11 7.8 1.47 0.6 (3)		D11R 3.9 1.60 0.9 (3)
				Ih							
					F14 2.0 2.88 $\Omega=2.6$ (5)		Z14R 3.9 1.12 1.0 (3)		D14RR 2.1 2.34 1.0 (3)		

Figure S1: Selected Pt₁₃ isomers, classified into their geometrical families. The left columns represents the gas phase (F prefixes), the middle column represents Pt₁₃ inserted into the zeolite supercage (Z prefixes); and the third column represents refinement at the DFT-D level (D prefixes). For each cluster, the total magnetisation in Bohr magneton (μ_B), the relative energy with respect the global minimum (in eV), and the solid angle at the anchor are listed below their identification label. The coordination of the anchor itself is listed in brackets.

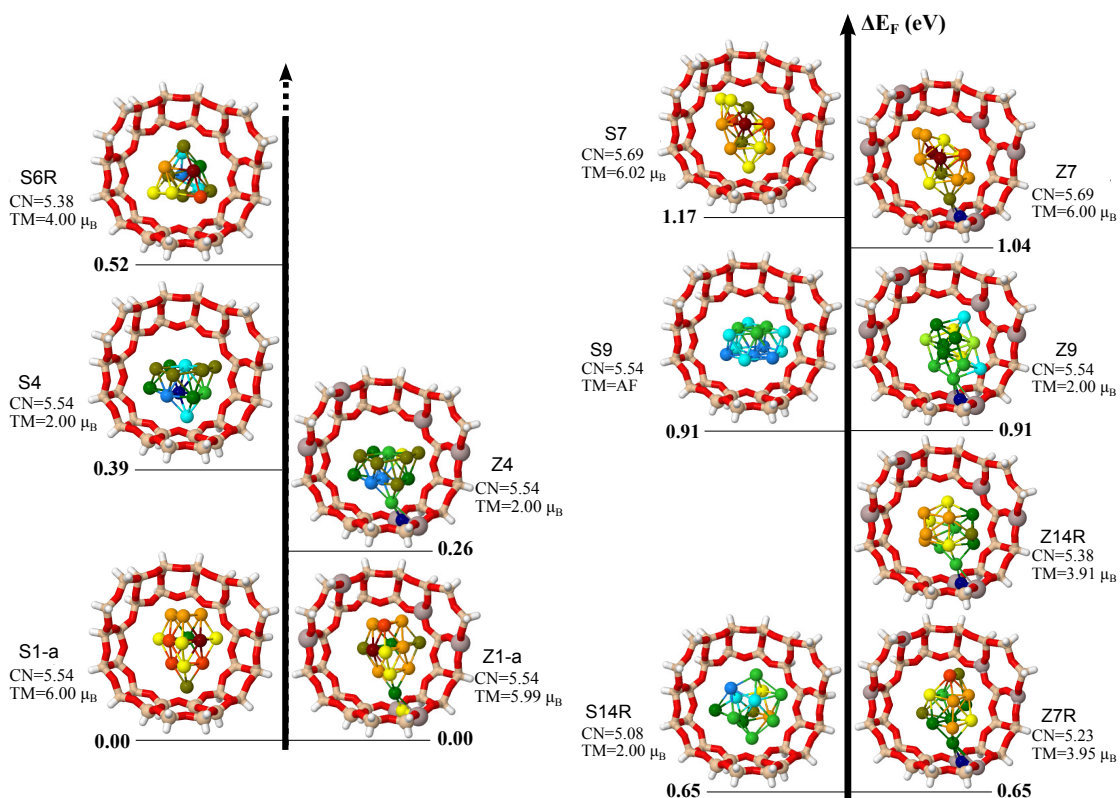


Figure S2: Energetic stability of Pt_{13} -NPs with respect to D1 embedded in a full silicon (left) and in an Al/Si NaY zeolite (right). Subscripts refer to the coordination of the anchor. The supercage is not magnetic, Si atoms are represented in light-orange; hydrogen in white; aluminium in grey; oxygen in red, with the exception of the anchor that is coloured to be consistent with the partial charge transfer with the Pt-vertex. Pt atoms are coloured according to their atomic polarisation calculated through a Bader algorithm.

insertion of the cluster in the non Löwenstein model cage produces structures with the overall lower energy probably because the bond within Pt and O is stronger and the cluster accommodates better in the cage. The breakdown of Lowenstein's rule is likely the result of the lack of periodicity and is thus also likely due to the Al atoms being trivalent. To better explore this last point, we have constructed another model zeolite, where all Al and Si atoms kept their original tetravalent coordination. Using the same theoretical tools as for the trivalent Al and Si cage, we have investigated the electronic charge distribution and the energy stability of each Si/Al ordering. Our conclusions are that the electronic charge remains essentially the same for the tetravalent or trivalent coordinations, and also the energetic stability shows that the Al-O-Si ordering is slightly preferable to the non Löwenstein ordering. However, simulation of the tetravalent model with the clusters is beyond our actual computational resources, but further investigation on these models is planned. We are currently exploring the validity of the Löwenstein's rule in a complete periodic structure with and without the inclusion of Pt_{13} clusters. This analysis cannot find space in this work.

Notably, the Si/Al model proposed here correctly reproduces the pair distance distribution function (PDDF) observed in experiments. This correlation should justify the shortening of the Pt-O bond length induced by a charge transfer that occurs only when two Al atoms are substituted for Si at site II of the supercage. An analysis of the PDDF, as averaged over all the considered structures, and reported in Fig. S3, reveals that the Pt-O mean distance in a full silicon cage, $\text{H}_{36}\text{O}_{42}\text{Si}_{30}$, is clearly far less than the 2.0 \AA . Other useful structural details as observed in experiments were reported in Ref. ¹³ Notably, the partial atomic charge transfer among Pt atoms of the NP remains essentially unaffected in both cases.

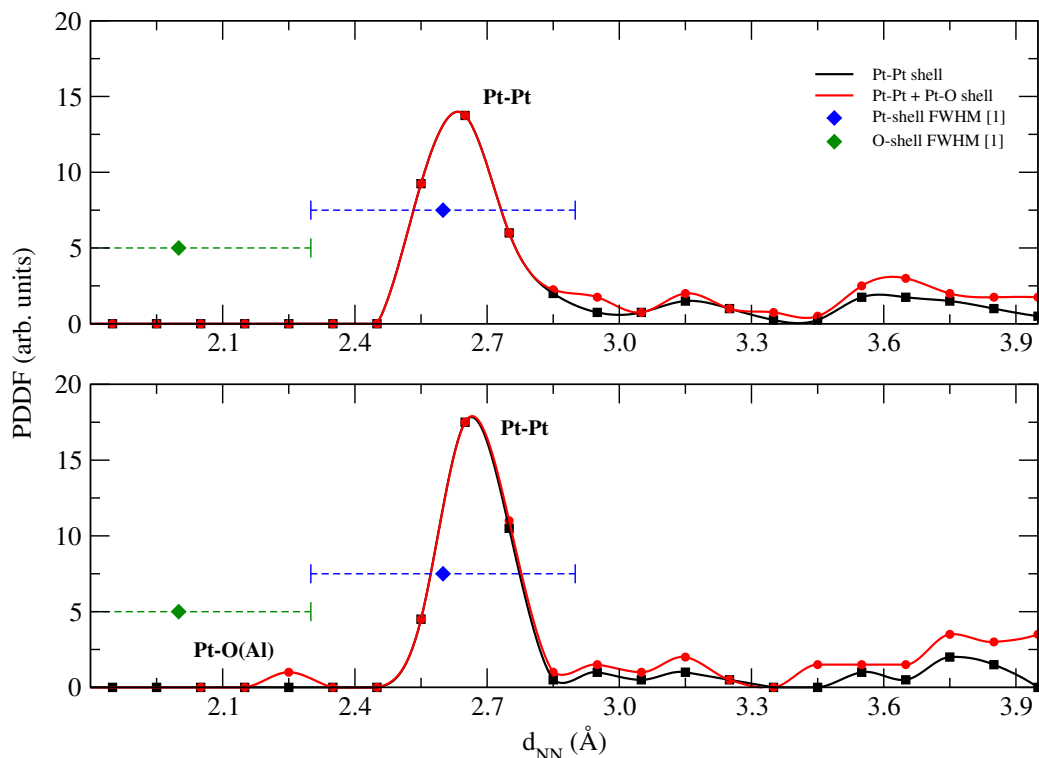


Figure S3: PDDF averaged over the considered Pt-NPs encapsulated in a faujasite supercage. Solid lines are only guides for the eye. Experimental values for the Pt-Pt and the Pt-O distance are estimated from the data of Liu et al. Ref. 12.

Geometrical description of selected isomers and their structural transformations at the DFT and DFT-D levels

All the selected clusters are reported in the first column of S1 and then they are grouped into their geometrical families. The classification is done on the basis of their Common Neighbour Analysis signature, as reported in detail in our previous work.³ A TBP, F1, an incomplete decahedron of 23 atoms (iDh_{23}) with no five-fold vertices, lies only 0.41 eV above the optimal F0. Three almost isoenergetic isomers exist in the range 0.7-0.9 eV: an incomplete double icosahedron of 19 atoms (iDh_{19} , labeled F5), two incomplete Dh_{23} , F3, and the so-called half-star (F4), which is a stellated iDh_{23} with only two tips. A three-fold symmetric TTP, tagged F2, lies 1.18 eV above F0. A bi-layer geometry (F9), which is the only fully crystallographic local minimum, is almost isoenergetic with F2. Seven high energy isomers, with a ΔE between 1.3 and 1.6 eV are F13, an iDh_{23} with a five-fold vertex; three helicoidal shapes (F8, F10, and F11); the so-called Dada-TTP (F6), which consists of a TTP of 9 atoms attached to Dh_7 showing a five-fold vertex; two incomplete iDh_{19} , the Dada-Ih (F7) and the F12.³ Finally, the Ih_{13} (F14) lies above 2.5 eV. The main effect of the embedding in a zeolite pore, is to destabilize all those shapes anchored throughout a fivefold vertex. As examples, we consider the Ih (F14) and the other isomers anchored through a five-fold coordinated vertex, such as the Dada-TTP (F6) and the Dada-Ih (F7). F14 and F6 indeed evolve towards iDh_{23} upon a three-fold anchor, Z14R is a very distorted Z4 and Z6R is similar to Z3, but with one atom arranged on an anti-Mackay site. F7 and F8, with five-fold anchors, reconstruct as poly-octahedra identified as Z7R and Z8R, respectively, with three tips anchored through a 4-coordinated vertex. A minor structural change happens for F13-5, showing a E_{enc} of 0.9 eV, but leading to a local reconstruction around the anchor, ZR13-3, around its anchor in order to get it 3-fold coordinated.

Among the stable geometrical motifs with a high TM and CN, the most energetically favorable is the truncated bipyramid, Z1, being only 0.4 eV above Z0-c. The same structural stability is observed for the iDh_{19} (Z5 and Z12) and the Dada-Ih (Z7), which are at 0.8, 1.26, and 1.44 eV above the global minimum, respectively. Helicoidal motifs Z8, Z10, and Z11, which are linked through a four-fold vertex, are stable but fairly high in energy ($\Delta E \sim 1.55$ eV).

Below, a detailed description of the structural transformations of Pt_{13} isomers within the DFT-D framework

is provided. With respect to the DFT level, about half of the considered isomers modify significantly their shape and almost all of them -with the exception of D1, D2 and D13R- present small distortions in order to decrease their overall coordination although their geometrical family is unchanged. Apart the structural transformation of global minimum, D0R-c, already described, those structures that reconstructed because of the embedding (i.e., Z6R, Z7R, Z8R, and Z14R), continue to change at the DFT-D level, where D6RR becomes a distorted D0R-a with a symmetry plane, D7RR is a stellated hexahedron plus a triangular prism, less coordinated than its parent Z7R, D8RR becomes very similar to D7RR, and D14RR is a slightly distorted D4. On top of those transformations, three isomers -Z6, Z10 and Z11- undergo to a structural change once dispersion forces are added -D6R*, D10R, and D11R. Notably, the Dada-TTP (D6R*) becomes an incomplete Dh₂₃ similar to D6RR but delimited by rhombic instead of square facets. D10R is now attached throughout a four-fold coordinated anchor and D11R is an incomplete hexagonal anti-prism with a defect and few square facets. Notably, isomers belonging to the iDh₂₃ family show small distortions at DFT-D level. Because of their larger gyration radius, the half-star, D4, is 0.4 eV more favourable than the stiffer D1, whose energy indeed decreases to 2.-2.5 eV above that of D0R-c, depending on the coordination of its anchor. Similarly, among idIh₁₉ clusters, the CN of D12 decreases from 5.3 to 4.7 and remains at 1.5 eV above D0R-c. In contrast, the more rigid D7 and D5 are still characterised by a high spin state and a CN close to 5.3; however, their ΔE are more than 2 eV greater than the global minimum.

Among the reconstructed structures, D0R-c, D8RR, and D13R preserve their TMs while D10R has a TM of 6 μ_B , D6RR, D8RR and D11R decreases to a TM of 4 μ_B , D6R*, D7RR, and D14RR exhibit a TM of 2 μ_B , as reported in Fig. 3.

Super atom model

Some of the magnetic behaviour of the Pt₁₃ loaded zeolite has been interpreted in terms of a super-atom model of the Pt₁₃ cluster.¹⁴⁻¹⁶ The idea that a cluster of atoms might form a super-atom structure, where the electrons are occupying highly degenerate states that could be labelled as in a standard atomic configuration has been proposed to explain the magic number behaviour of some Na clusters and then generalised to other clusters.^{16,17} As suggested by those same authors, the idea works best when the clusters maintain a high level of degeneracy (ideally then a icosahedral motif), since it allows the electrons to occupy highly degenerate states that can be labelled using the standard quantum numbers of the atomic structure. Then one can discuss the presence of open and closed shell, the role of the spin pairing energy and so on. We have attempted an analysis of our clusters using this powerful unifying idea, but we realised that our low symmetry structures do not allow for the high degeneracy necessary for a super-atom description (some of the high symmetric structure in the gas phase do have some level degeneracy). Moreover, when embedded in the zeolite cage, the symmetry is further reduced by the presence of the anchor and the super-atom is not useful. We have also investigated the character of the highest occupied molecular orbital as calculated from the Kohn-Sham states obtained from Quantum Espresso, see Fig. S4. We see that this state is partially hybridised with the cage, while it does not necessarily belong to the spin majority series. To further analyse the properties of our clusters, we have studied the spin-resolved energy-level distribution for the relaxed cluster in the gas phase via a DFT calculation. We report our result in Fig. S5 for the case of F0, F14, and F21. From the figure, one can clearly see that the energy levels for the F0 and F2 due to their reduced symmetry, are almost non-degenerate and there is a consistent shift between the level of the majority and minority spins. Some of the levels also seem clustering, suggesting that the lack of symmetry produces a small splitting energy. For those clusters, a super-atom model is not really informative and the concept of shell not relevant. For the case of the Ih, F14, we observe a more consistent degeneracy of the levels (although some of them also show a small energy splitting) suggesting that a super-atom model can offer some insight of the chemical and physical properties of this cluster.

References

- [1] A. Laio and M. Parrinello, *Proc. Natl. Acad. Sci. U.S.A.*, 2002, **99**, 12562.
- [2] G. A. Tribello, J. Cuny, H. Eshet and M. Parrinello, *J. Chem. Phys.*, 2011, **135**, 114109.
- [3] L. Pavan, C. Di Paola and F. Baletto, *Eur. Phys. J. D*, 2013, **67**, 24.
- [4] V. Rosato, M. Guillopé and B. Legrand, *Philos. Mag. A*, 1989, **59**, 321.

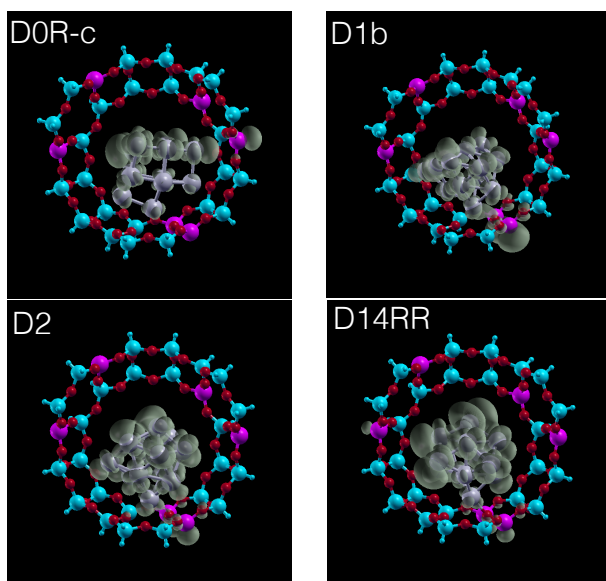


Figure S4: Density of the Kohn-Sham homo state (in dark green) as obtained from Quantum Espresso. In grey the platinum atoms, within the zeolite cage model (red, cyan, and purple). Notice that the homo state is not necessarily belonging to the majority spin sequence.

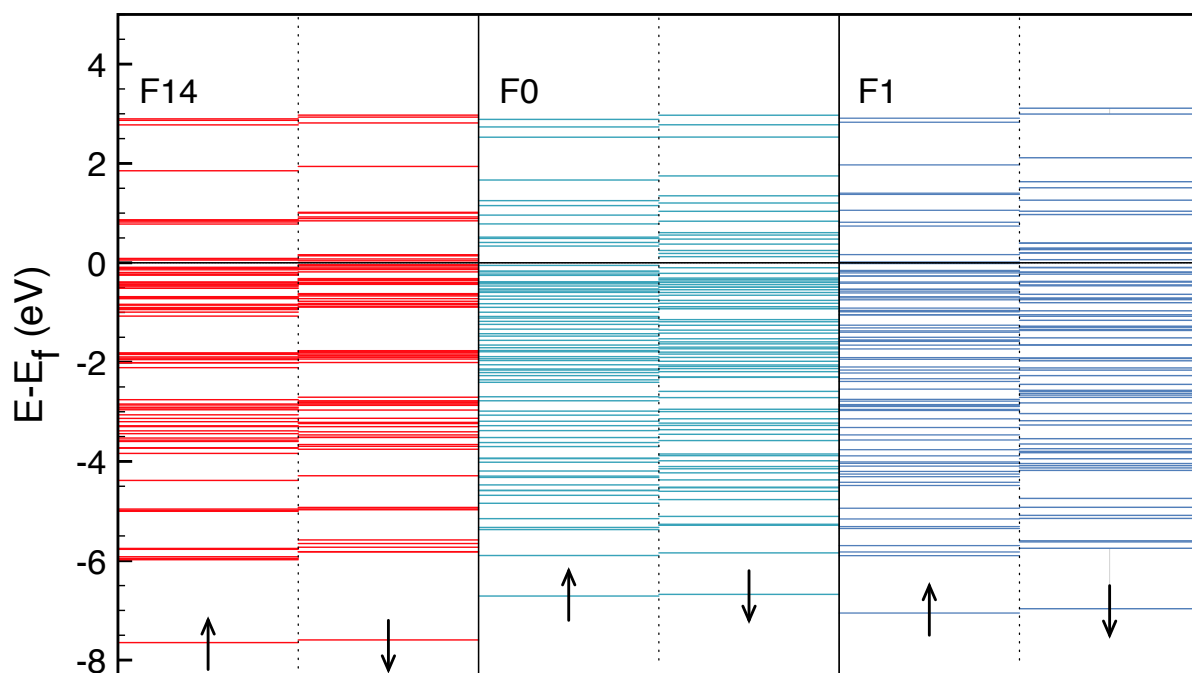


Figure S5: Spin-resolved energy level distribution for the F14 (left), F0 (center), and F1 (right) Pt_{13} clusters, as obtained from a DFT calculation of the relaxed structure in the gas phase. All the levels are shifted with respect to the highest occupied energy level.

- [5] P. Giannozzi, S. Baroni, N. Bonini, M. Calandra, R. Car, C. Cavazzoni, D. Ceresoli, G. L. Chiarotti, M. Cococcioni, I. Dabo, A. Dal Corso, S. de Gironcoli, S. Fabris, G. Fratesi, R. Gebauer, U. Gerstmann, C. Gougoussis, A. Kokalj, M. Lazzeri, L. Martin-Samos, N. Marzari, F. Mauri, R. Mazzarello, S. Paolini,

- A. Pasquarello, L. Paulatto, C. Sbraccia, S. Scandolo, G. Sciauzero, A. P. Seitsonen, A. Smogunov, P. Umari and R. M. Wentzcovitch, *J. Phys. Condens. Matter*, 2009, **21**, 395502.
- [6] P. Blonski and J. Hafner, *J. Phys.-Condens. Matter*, 2011, **23**, 136001.
- [7] N. Marzari, D. Vanderbilt, A. De Vita and M. C. Payne, *Phys. Rev. Lett.*, 1999, **82**, 3296.
- [8] C. Di Paola and F. Baletto, *Proceedings for CMMSE XI*, 2011, **2**, 451.
- [9] V. Barone, M. Casarin, D. Forrer, M. Pavone, M. Sambi and A. Vittadini, *J. Comput. Chem.*, 2009, **30**, 934–939.
- [10] E. Roduner, C. Jensen, J. van Slageren, R. A. Rakoczy, O. Larlus and M. Hunger, *Angew. Chemie - Int. Ed.*, 2014, **53**, 4318–4321.
- [11] R. Bell, R. Jackson and C. Catlow, *Zeolites*, 1992, **12**, 870.
- [12] X. Liu, M. Bauer, H. Bertagnolli, E. Roduner, J. van Slageren and F. Phillipp, *Phys. Rev. Lett.*, 2006, **97**, 253401.
- [13] P. Gallezot and G. Bergeret, in *Catalyst deactivation*, ed. E. Petersen and A. Bell, Dekker, 1987, p. 263.
- [14] C. Jensen, D. Buck, H. Dilger, M. Bauer, F. Phillipp and E. Roduner, *Chem. Commun.*, 2013, **49**, 588–590.
- [15] C. Jensen, J. van Slageren, P. Jakes, R. A. Eichel and E. Roduner, *J. Phys. Chem. C*, 2013, **117**, 22732–22745.
- [16] E. Roduner and C. Jensen, *Magnetochemistry*, 2015, **1**, 28–44.
- [17] A. Castleman and S. Khanna, *J. Phys. Chem C*, 2009, **113**, 2664–2675.